# Ionospheric Correction by Means of Coherent Scatterers

Rafael Zandoná-Schneider, Konstantinos Papathanassiou
German Aerospace Center (DLR), HR-Institute, Wessling, Germany

## Abstract

The operation of low frequency SAR sensors on space-borne platforms is perturbed by the presence of Earth's ionosphere. The purpose of this paper is to outline an initial methodology exploiting the potential of Coherent Scatterers (CSs) for the estimation and correction of the different effects induced by ionospheric disturbances on SAR images. Based on the high spectral correlation and the point-like scattering behavior that characterize CSs, we discuss and propose the estimation and compensation of different ionospheric effects, and assess their performance by using real SAR data and simulated ionospheric disturbances.

## 1 Introduction

The lower the operating frequency of a SAR sensor, the more susceptible it becomes to ionospheric disturbances.
The ionosphere affects the (band-limited) signal transmitted/received by the SAR system in different ways [1]:

- The electron density (given by the actual density profile or approximated by the total electron content - TEC) along the signal path introduce group delay, dispersion and Faraday rotation;
- Electron density irregularities induce signal scintillation through narrow-angle forward scattering.

The scintillation cause temporal and/or spatial fluctuations in signal amplitude, phase, polarization or angle-of-arrival. Such phase scintillation limit the correlation length of the medium.
As a matter of fact, the ionosphere affects all individual (wave) parameters of the transmitted/received pulses, i.e. the amplitude (attenuation, Faraday rotation), the phase (delay, dispersion, scintillation) as well as propagation velocity and direction. In consequence, the ionosphere may constrain significantly the performance of the SAR instrument.
There are five main distortions introduced by the ionosphere on the images obtained by a low frequency SAR:

- Range timing errors caused by propagation phase distortion (group-delay) that translate to positioning errors;
- Range de-focussing caused by dispersion within the pulse-bandwidth;
- Azimuth de-focussing due to high frequency phase distortion along the integration path (phase scintillation);
- Polarization mismatch due to the Faraday rotation.
- Phase bias due to the temporal variation of the ionosphere in repeat-pass InSAR acquisitions.

In this paper, we exploit the potential of point-like scatterers - the so called coherent scatterers (CSs) [2], for the mitigation of ionospheric induced errors in SAR images. The high spectral correlation that characterizes the CSs is essential for the estimation of dispersion effects, while at the same time, the potential to detect CSs on the basis of a single image provides the possibility for absolute estimation. We discuss here the potential of CSs for the mitigation of the four first above mentioned distortion effects.

## 2 Coherent Scatterers (CSs)

When dealing with point scatterers, several advantages arise, if compared to distributed scatterers, due to their deterministic scattering behavior, in contradiction to the random nature of distributed scatterers in SAR images.
Recently, the Coherent Scatterers technique has been proposed in order to detect point-like scatterers in SAR images [2]. The deterministic scattering behavior of point scatterers implies their very high spectral correlation. The CSs technique exploit this property, by detecting the resolution cells having high sublooks spectral correlation.
In agreement with the expected characteristics of point scatterers, it has been shown in [2] that the great majority of CSs have high amplitude, very high interferometric coherence and low polarimetric entropy (high polarimetric coherence). This potentially suggests the application of CSs in several fields, as for example, for radiometric and polarimetric calibration purposes, phase deviations correction, for general interferometric and polarimetric applications, etc. In this paper we specifically address the utilization of CSs for the correction of different ionospheric induced effects in SAR images acquired at low frequencies.

## 3 Azimuth de-focussing

An important ionospheric effect is the spatial influence on the signals going through the ionosphere, originating high frequency phase distortions on signals spatially separated. Such effect is called phase scintillation, and will affect the

azimuth signals when collecting the data within the synthetic aperture, causing azimuth de-focusing in the SAR processed image.

A possible idea is hence to perform an azimuth autofocus procedure, using as basis scatterers having an expected stable phase along the azimuth aperture. For spaceborne systems, having a narrow azimuth angular variation, CSs are expected to have such phase stability and may be used as reference scatterers for the autofocus procedure.

When a certain amount of such scatterers in a given region of a SAR image present a common phase variation along the azimuth aperture, such variation may be associated to the ionospheric induced phase scintillation and can be estimated and compensated.

The applied autofocus procedure has been the Phase Curvature Algorithm (PCA) [3], which is the stripmap version of the spotlight Phase Gradient Algorithm (PGA) [4]. As the name suggests, the PCA is able to recover phase curvatures but not linear phase errors. In the original algorithm, the estimation of the phase errors are performed using the scatterers with highest amplitude in every range line, due to their larger Signal to Clutter Ratio. In our case instead, we use the set of detected CSs in the scene as the reference scatterers for the phase error estimation.

We verify the performance of ionospheric phase error correction using this CSs based autofocus, by applying a simulated ionospheric phase error on a real SAR image, followed by its estimation and comparison with the original one. Firstly, a one-dimensional (azimuth) phase error is applied, being common to the whole range dimension. In a second step, a two-dimensional phase error is applied, for which more difficulties are expected due to the lower number of CSs sharing the same phase error along the range direction. The used SAR image has been acquired at L-band by the E-SAR system of the German Aerospace Center over the city of Munich in Germany. The ionospheric phase disturbances have been simulated under typical conditions.

### 3.1 One-dimensional phase error

**Figures 1(a)** and **1(b)** show two phase errors inserted in the de-focused SAR image, and the recovered ones after the azimuth CSs autofocus. The recovered phase has been evaluated after just one iteration of the autofocus procedure.

Note that although just a single iteration has been performed, already a high agreement between the original and estimated phase errors has been obtained. There is a set of parameters which influence the algorithm performance that has to be chosen in the autofocus procedure. The improvement of the phase error estimation is thus possible, when the optimal parameters are selected for a given situation.

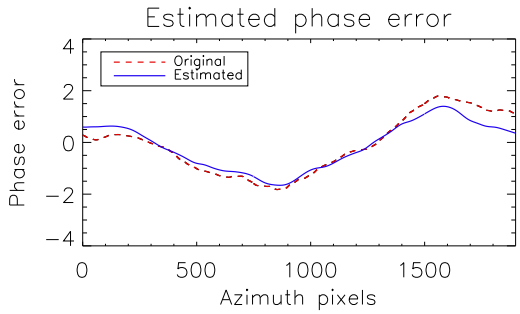


(a) One-dimensional phase error example 1

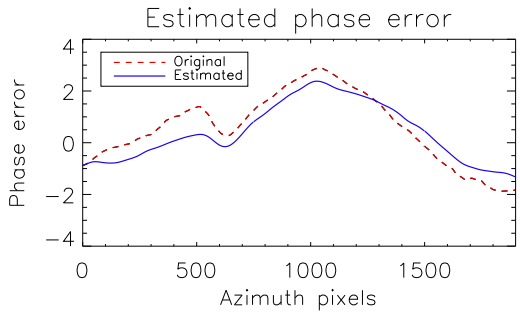


(b) One-dimensional phase error example 2

**Figure 1:** Estimated one-dimensional azimuth phase errors after one iteration of the autofocus procedure.

### 3.2 Two-dimensional phase error

The two dimensional phase error used here has been generated by gradually varying (in range) the values between two one dimensional simulated azimuth phase errors, located at the extremes of the 2D phase error. The objective is to have an idea of the algorithm performance when variation along the range direction is also present.
**Figure 2(a)** shows the 2D phase error inserted in the de-focused SAR image, while **Figure 2(b)** presents the estimated 2D phase and **Figure 2(c)** the corresponding RMS error between them. Also in this case the recovered phase has been evaluated after just one iteration of the autofocus procedure.
As could be expected, the performance is inferior for the 2D case, although a still reasonable agreement between the original and estimated phase errors has been obtained, after a single iteration.

## 4 Range de-focusing

Ionosphere disturbances as phase dispersion along frequencies affect the range response of SAR systems causing range de-focusing. CSs are expected to have their phase widely stable along the frequency domain. A similar autofocus procedure in the range direction, as the one in azimuth, is thus an alternative in order to estimate and com-

pensate the phase variations induced by ionospheric dispersion along the frequencies of the SAR bandwidth.
Although the autofocus in range has not been implemented in this work, we would like to demonstrate the CSs phase stability along frequencies, which is a necessary condition, and suggests a good performance, in an autofocus procedure.
**Figures 3(a)** and **3(b)** present two examples of phase variation of CSs along the frequencies of the system bandwith, which have been obtained through the evaluation of several range sublook images. **Figure 3(c)** shows an example of the phase variation along frequencies of a general distributed scatterer. Note the strong phase stability of CSs with the variation of the frequency, what indicates also their potential for range de-focusing correction.

# 5 Range timing errors

The phase of a point scatterer for different sublook images centered at the frequencies $f_i$ may be expressed as [5]

$$\phi = 2\pi(f_i - f_0)t - \frac{4\pi}{c} f_i R + \phi_s \qquad (1)$$

where $t$ is the range time, $R$ is the scatterer range position, $c$ is the light velocity, $f_0$ the system central frequency and $\phi_s$ the scatterer phase due to the scatterer properties, which for CSs is frequency independent. Hence, the phase ramps observed in **Figures 3(a)** and **3(b)** are in fact originated from the difference between the nominal (sampled) $R_N = ct/2$ and the actual $R$ range position of the CS

$$\phi = \frac{4\pi}{c} f_i (R_N - R) - \frac{4\pi}{c} f_0 R_N + \phi_s. \qquad (2)$$

It is thus possible to retrieve the scatterer absolute range distance through the inclination slope of the phase curve, i.e., the derivative of the phase in relation to the frequency

$$R_N - R = \frac{c}{4\pi}\frac{\partial\phi}{\partial f_i} = \frac{c}{4\pi}\frac{1}{|S|^2}\Im\left\{\frac{\partial S}{\partial f}\cdot S^*\right\} \qquad (3)$$

where $S$ is the complex scatterer signal, $\Im\{\cdot\}$ means imaginary and $^*$ complex conjugate. Using the above equation the range differences encountered for the examples of **Figures 3(a)** and **3(b)** are $0.70\,m$ and $-0.45\,m$, respectively. Note that phase wrapping in frequency will for practical situations be not a problem at all when using (3). The phase would wrap just if its variation from one sublook to the next reaches $2\pi$. However, as typical pixel distances in frequency are in general in the order of $kHz$ (for the E-SAR system about $70\,kHz$), sublook images can be generated using this step and a difference in the nominal to the actual CS range position should be larger than $2\,km$ for wrapping, what is unrealistic.
This accurate determination of the range position of CSs may also be exploited in order to observe the range timing errors caused by the ionosphere, suggesting another potential application of CSs for the reduction of ionospheric effects in SAR images.

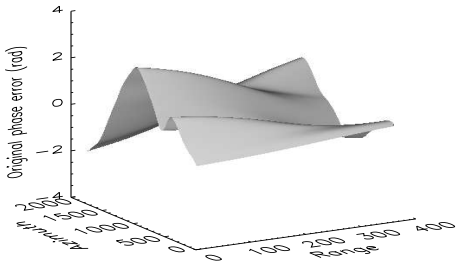


(a) Original two-dimensional phase error

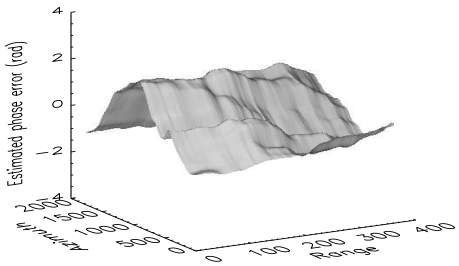


(b) Estimated two-dimensional phase error

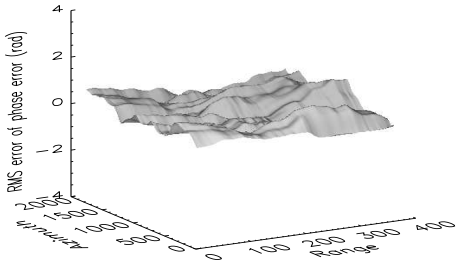


(c) RMS error of the two-dimensional phase estimation

**Figure 2:** Two-dimensional autofocus after one iteration.

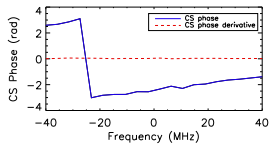


(a) CS phase and phase derivative

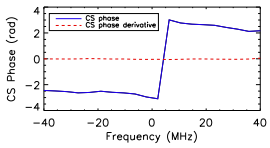


(b) CS phase and phase derivative

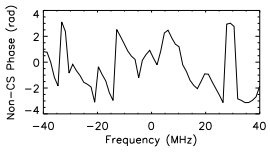


(c) Distributed scatterer phase

**Figure 3:** Example of phase and phase derivative as a function of frequency, for two CSs and a Non-CS scatterer.

### 5.1 Alternative selection of CSs

Using equation (3) an alternative detection of phase stable scatterers, as CSs, may be performed. Defining the mean $m$ and variance $\sigma^2$ of the phase derivative with respect to frequency for $N$ sublooks as

$$m = \frac{1}{N}\sum_{i=1}^{N}\frac{\partial\phi_i}{\partial f} \quad \text{and} \quad \sigma^2 = \frac{1}{N}\sum_{i=1}^{N}\left(\frac{\partial\phi_i}{\partial f} - m\right)^2 \quad (4)$$

one may use the ratio $r = \sigma/m$ as a measure of phase stability along frequencies and select scatterers in a SAR image having $r$ lower than a given threshold. The advantage of this method is that no boxcar window needs to be used, as in the estimation of the sublooks coherence in [2], making possible a pixel-based detection. The disadvantage is the lost in range resolution if narrow bandwidth sublooks are used, and the computational time that is longer due to the generation of several sublooks.

## 6 Faraday rotation

In order to illustrate the potential of CSs for the estimation of the Faraday rotation effect in SAR images, two experiments have been carried out. The Faraday rotation angle has been estimated over the city of Munich using the data of two SAR sensors: the airborne system of DLR, and the spaceborne ALOS/PalSAR system, both at L-band. In the first case, no Faraday rotation is expected since the data was acquired by an airborne system.
The Faraday rotation angle $\Omega$ has been estimated by

$$\Omega = \frac{1}{2}\arctan\left\{\frac{S_{HV} - S_{VH}}{S_{HH} + S_{VV}}\right\}. \quad (5)$$

**Figure 4(a)** presents the histograms of the Faraday rotation estimation in the E-SAR data, using the detected CSs and for Non-CS scatterers. **Figure 4(b)** shows the corresponding histograms for the the ALOS/PalSAR system.
Observe that for both cases the estimation of Faraday rotation using CSs is more accurate, having less dispersion of values around the true value, when compared to the Faraday angle estimation using Non-CS scatterers. As expected, the Faraday rotation over Munich using the E-SAR system is zero. On the other hand, a Faraday rotation angle of almost 1 degree can be observed in the PalSAR data, which can be better identified in the CSs estimation.

## 7 Conclusions

In the paper, the potential of CSs to mitigate the different undesired ionospheric effects which originate in SAR images acquired by spaceborne systems at low frequencies has initially been outlined. The obtained results from this first analysis have shown that the potential for the mitigation of most of the effects exist, however further work has to be carried out in order to improve and validate the obtained estimation of some effects and to develop estimation strategies for the other ionospheric disturbances in SAR images.

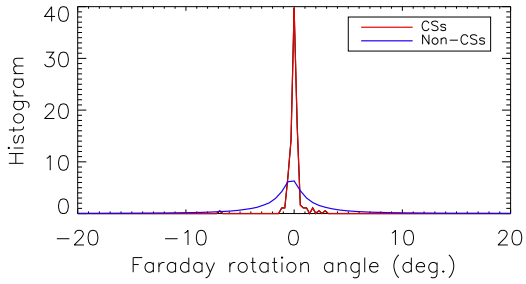


(a) Airborne E-SAR system

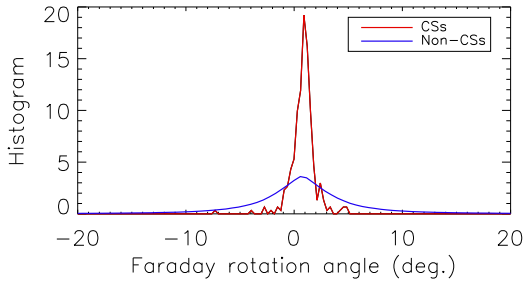


(b) Spaceborne ALOS system

**Figure 4:** Faraday rotation estimation over Munich: airborne E-SAR and spaceborne ALOS system.

## References


[1] Z. W. Xu, J. Wu, and Z.-S. Wu: *A survey of ionospheric effects on space-based radar*, Waves in Random Media, 14, S189-S273, 2004.

[2] R. Zandona-Schneider, K. P. Papathanassiou, I. Hajnsek, A. Moreira: *Polarimetric and Interferometric Characterization of Coherent Scatterers in Urban Areas*, IEEE Trans. Geoscience and Remote Sensing, vol. 44, No. 4, pp. 971-984, April 2006.

[3] D. E. Wahl, C. V. Jakowatz, Jr.; P. A. Thompson, and D. C. Ghiglia: *New approach to strip-map SAR autofocus*, Digital Signal Processing Workshop, pp. 53-56, 2-5 October 1994.

[4] P. H. Eichel, D. C. Ghiglia, and C. V. Jakowatz, Jr.: *Speckle processing method for synthetic-aperture-radar phase correction*, Optics Letters, vol. 14, No. 1, pp. 1-3, January 1989.

[5] N. Veneziani, F. Bovenga, and A. Refice: *A Wideband approach to the absolute phase retrieval in SAR interferometry*, Multidimensional Systems and Signal Processing, vol. 14, Issue. 1-3, pp. 183-205, 2003.